Journal of Applied Polymer Science

Functionalization of Polyvinyl Alcohol Hydrogels with Graphene Oxide for Potential Dye Removal

Chengpeng Li,[1,2] Mary She,[1] Xiaodong She,[1] Jane Dai,[1] Lingxue Kong[1]
[1]Institute for Frontier Materials, Deakin University, Waurn Ponds, Victoria 3216, Australia
[2]College of science, Guangdong Ocean University, Zhanjiang, Guangdong, Peoples' Republic of China
Correspondence to: L. Kong (E-mail: lingxue.kong@deakin.edu.au)

ABSTRACT: Because of highly frozen macromolecule chains, polyvinyl alcohol (PVA) hydrogels have never been used for dye removal. This work focuses on improving the adsorption capacity of the PVA hydrogel by using amphiphilic graphene oxide to improve its macromolecular chain mobility in crystal domain and introduce new functional groups. To evaluate its effectiveness, crystal structure, swelling kinetics, and model dye methylene blue (MB) adsorption of the as-prepared PVA hybrid hydrogels were systematically investigated. The results indicate that the hybrid PVA hydrogels have lower crystallinity and less crystal stability, demonstrating the improved macromolecular chain mobility. Moreover, improved swelling ratios of PVA/GO hydrogels also illustrate the enhanced macromolecular chain mobility. MB adsorption experiment indicates that GO introduced can result in great improvement in MB adsorption. And the adsorption process follows the second-order kinetic model and Morris–Weber model, which is determined by the intraparticle diffusion. Furthermore, MB adsorption isotherm follows Freundlich model and the adsorption is heterogeneous. Desorption studies indicate that the interaction between PVA hydrogels and MB consists of both physisorption and chemisorption.
 J. Appl. Polym. Sci. **2013**, *000*, 39872.

KEYWORDS: adsorption; gels; kinetics

Received 27 May 2013; accepted 21 August 2013
DOI: 10.1002/app.39872

INTRODUCTION

Poly (vinyl alcohol) (PVA) is a kind of biocompatible and biodegradable polymers with three kinds of tacticities: syndiotacticity, isotacticity, and heterotacticity. It has been widely used to prepare functional hydrogels for pharmaceutical applications.[1–3] Especially, PVA hydrogel can be prepared by the common freezing/thawing cycle without the use of traditional chemical crosslinking techniques that are widely used in other hydrogel preparation,[4,5] because physical crosslinking can be formed in concentrated PVA solution via numerous crystalline areas. Hydrogels, except PVA hydrogel, have been widely applied for numerous dye removals.[6,7] However, the potential of using PVA hydrogel for dye removal has not been explored till now, because of its frozen molecule chains and lack of functional groups (only hydroxyl groups existed). Therefore, optimization of molecular interaction and introduction of functional groups in PVA hydrogels become extremely meaningful both theoretically and practically in expanding PVA hydrogel application for dye removal.

Both physical blending and chemical modification can be used to change molecular interactions and produce functional groups. However, chemical modification of PVA macromolecules may lead to the great change of PVA molecular structure and failed gelation (freezing/thawing cycle). Polymer composite is a versatile research direction for physical blending. Especially, the interface between nanosized fillers and polymer matrix makes it possible for the fillers to interact with matrix effectively and acquire good performances such as high stiffness, transparency, and flame retardance.[8]

Graphene, a two-dimensional carbon material, has been widely explored in polymer composite fabrication because of its huge surface area, good conductivity, and high strength.[9] However, the dispersion concentration of graphene is extremely low.[10] Graphene oxide (GO), as an important precursor for graphene, possesses good dispersion,[11,12] high specific surface,[13] and abundant functional groups such as hydroxyl, epoxy, carbonyl, and carboxyl groups.[14] More important, recent research showed that GO can be used as an effective absorbent for Cu^{2+},[11] arsenic,[15] and MB because of its high specific surface and abundant active groups.[16]

In this article, amphiphilic GO with high surface area and good dispersion was introduced in PVA hydrogels for functionalization. The adsorption ability of the as-prepared hydrogels was evaluated with a cationic dye methylene blue (MB). Our

strategy here is to use amphiphilic GO to weaken the strong intramolecular and intermolecular hydrogen bonds and improve the mobility of PVA molecular chains within the crystal domain in PVA hydrogels. This idea is totally different from the common composite fabrication strategy that aims at improving the interface interaction.[17,18] To our best knowledge, it is the first exploration of GO/PVA hybrid hydrogels as a dye remover, which may enhance the understanding of PVA/GO hybrid materials and expand their potential applications.

EXPERIMENTAL

Materials

PVA (Mw ~145,000, hydrolysis degree 98–99%), Graphite (particle size <45 μm), potassium permanganate and hydrogen peroxide were all purchased from Sigma Aldrich (Sydney, Australia).

GO Synthesis

GO was synthesized from natural graphite by a modified Hummers method.[19] The as-synthesized GO was purified by dialysis in deionised water for 8 days to get a homogeneous solution. To get the accurate concentration of GO, 100 g as-obtained GO solution in a known weight beaker was dried in an oven at 110°C for three days to remove all the water inside. The final weight of the beaker was checked again to get the residue weight of dried GO in 100 g GO solution. After that calibration, the as-prepared GO solution is concentrated to get 0.3 wt % dispersion for later application.

PVA Hydrogel Preparation

Aqueous solutions of 14 wt % PVA were prepared by dissolving PVA in deionised water for 6 h at 95°C, which were then mixed with GO solution or water with stirring. The as-prepared PVA/GO mixtures were cast into a plastic box and then exposed to freezing for 20 h at −20°C and thawing for 4 h at 22°C.[4] After five cycles, PVA hydrogels were formed. Three hydrogels with 0%, 0.3%, and 0.6% GO are designated as sample H-1, H-2, and H-3, respectively.

Characterizations

The X-ray powder diffraction (XRD) profiles of graphite and GO were obtained with a Phillips PW-1729 difractometer (35 kV, 28 mA) (Amsterdam, The Netherlands) with Cu$K\alpha$ radiation ($\lambda = 0.154$ nm) in the range of $2\theta = 5$–65° (by steps of 0.05°). The tube voltage and tube current were kept at 40 kV and 30 mA, respectively.

The morphology of GO and graphite was investigated by using scanning electron microscopy (Carl Zeiss AG SEM Supra 55VP). Before the investigation, all the samples were coated with gold.

The tacticity of the PVA was obtained by using ^{1}H NMR. It was conducted on a JEOL JNM-GX NMR instrument (270MHz) by dissolving PVA in deuterated dimethyl sulfoxide.

The XPS spectra was used to detect chemical structure of GO on a K-Alpha X-ray photoelectron spectrometer from Thermo Fischer Scientific using monochromatic x-rays focused to a 400 μm spot size. Excessive charging of the samples was minimized using a flood gun. The C1s binding energies of the GO were accurately established by charge shift correcting the lowest binding energy peak of the C1s to 284.6 eV. Survey spectra were obtained at a pass energy of 100 eV, whereas high resolution peak scans were performed at a 20 eV pass energy. The peak scans were employed to obtain the composition in terms of elements C and O.

Differential scanning calorimeter (DSC) was used to analyze the glass transition temperature and the crystallinity of the as-prepared hydrogels. The experiment was carried out using a TA-DSC model Q200 instrument. 15 ± 1.0 mg of hydrogel samples were used under nitrogen gas. To get the crystallinity, the samples were heated to 240°C at a rate of 15°C/min, which were then kept at 240°C for 5 minutes and finally cooled to 30°C at 20°C/min. The glass transition temperature was obtained from the second heating cycle (15°C/min).

Swelling Measurement

Hydrogel swelling ratio was determined by a gravimetric method. Hydrogel disks (around 1.80 cm in diameter and 0.40 cm in height) were immersed in distilled water (400 mL) at 25°C. The swollen samples were then weighted at predetermined time till the weights reached swelling balance. The swelling ratio was measured:

$$\text{Swelling ratio} = W_2/W_1 \quad (1)$$

where W_1 and W_2 are the weights of the original and the swollen hydrogels, respectively.

MB Adsorption and Desorption

Before adsorption experiment, a series of diluted MB solution was prepared with distilled water and was analyzed by using a UV spectrophotometer (Shimadzu UV-260) at the 662 nm.[20] The obtained calibration curve of MB is $C = -0.0044 + 4.20 \times A$ ($R = 0.998$, $0.077 \leq A \leq 0.91$), where C (mg/L) is the concentration of MB and A is the absorbance of MB. For the adsorption isotherm study, 1.00 ± 0.01 g hydrogel adsorbent was added into a 100mL vial containing 20.00 ± 0.01 g MB solutions. The initial MB concentrations for adsorption isotherm study are 164.4, 661.5, 749.1, 820.0, 927.9, and 1035.7 ppm, respectively. The adsorption was allowed to last for consecutive 4 days at 25°C to reach equilibrium. The amount of dye absorbed (μg/g) (q_t) on the hydrogels can be calculated from the mass balance equation as follows:

$$q_t = V(C_0 - C_e)/W \quad (2)$$

where V is the volume of MB solution, C_0 and C_e are the initial and final concentrations of MB in the solution. For adsorption kinetics study, a series of standard MB solutions containing 20.00 ± 0.2 mL MB were allowed to contact with 1.00 ± 0.01 g hydrogel at 20°C and 25°C, respectively. The concentration of the standard MB solutions is 3.45 ppm. At predetermined time intervals, the hydrogels were taken out and the solution was analyzed at the 662 nm. The amount of dye adsorbed (mg/g) (q_t) on the hydrogels can be calculated from eq. (2).

For desorption experiment, all the samples (1.00 ± 0.01g) were added into a 100 mL vial containing 20.00 ± 0.01 g MB solutions (1000 ppm) for consecutive 4 days at 20°C to reach equilibrium. After that, all samples were then taken out and washed

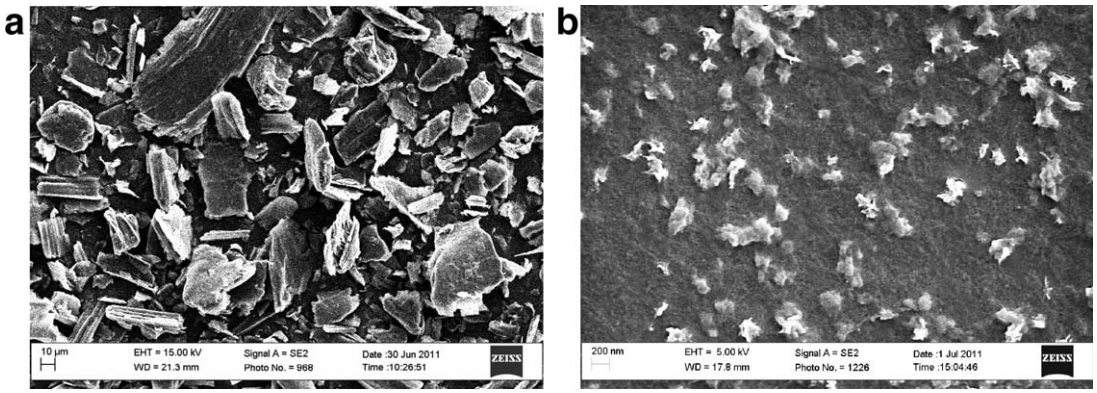

Figure 1. Electronic microscope images: (a) graphite; (b) graphite oxide.

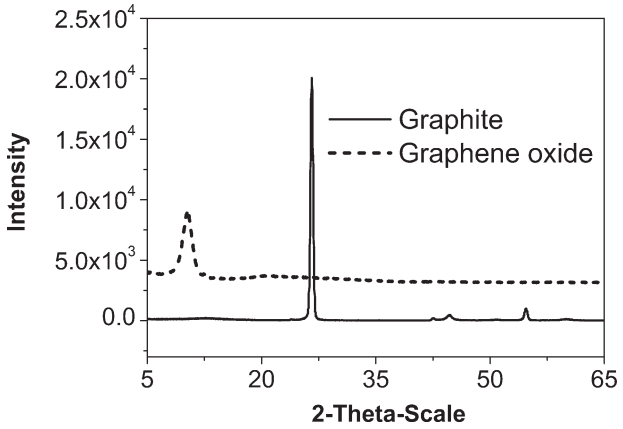

Figure 2. XRD patterns of graphite and GO.

gently with water to remove any unadsorbed MB. Finally all the hydrogel samples were suspended in 20.00 ± 0.01 g deionized water for predetermined time to investigate the desorption efficiency. The desorption efficiency can be determined by the following equation:

$$\text{Desorption efficiency}\,(\%) = \frac{\text{dye desorbed}}{\text{dye adsorbed}} \times 100\% \qquad (3)$$

RESULTS AND DISCUSSION

The morphologies of graphite and the as-prepared GO are shown in Figure 1. The size of GO is decreased greatly to about 300 nm [Figure 1(b)] from its original graphite of around 20 µm [Figure 1(a)], indicating the as-prepared GO is successfully exfoliated.[13] XRD patterns of pristine graphite and GO are shown in Figure 2. The peak (002) for graphite shifts from 26.7° to 10.3° after oxidation and exfoliation, demonstrating a great increase in the interlayer distance.[21]

The chemical composition of GO is obtained from XPS spectrum (Figure 3). Survey spectrum [Figure 3(a)] clearly shows the elements of carbon and oxygen. The asymmetric shape of the peak in C1s spectrum [Figure 3(b)] indicates the expected presence of an oxygen contribution. Quantitative information on the oxygen functionalities in the GO has been obtained from deconvolution of spectrum. The carbon oxygen ratio is 2.8 : 1. The first component in carbon is carbon sp^2 with a bonding energy of 284.6 ± 0.2ev. The second one is at 286.8 ± 0.2ev, which is attributed to epoxy/hydroxyl groups (C-O). The third component is carbonyl and carboxylates (C=O and O-C=O) with a bonding energy of 288.6 ± 0.2ev.[22] The as-prepared GO contains 70% and 30% of graphitic carbon and oxidized carbon, respectively, as calculated from the peak area. The remained graphitic carbon domain is contributed to the hydrophobic property, whereas the as-produced oxidized carbon domain is contributed to the hydrophilic property. Therefore, the as-prepared GO is amphiphilic.

As a kind of physical hydrogels, PVA hydrogels are joined together by both intermolecular and intramolecular hydrogen bonds.[23] These strong inner interactions are determined by

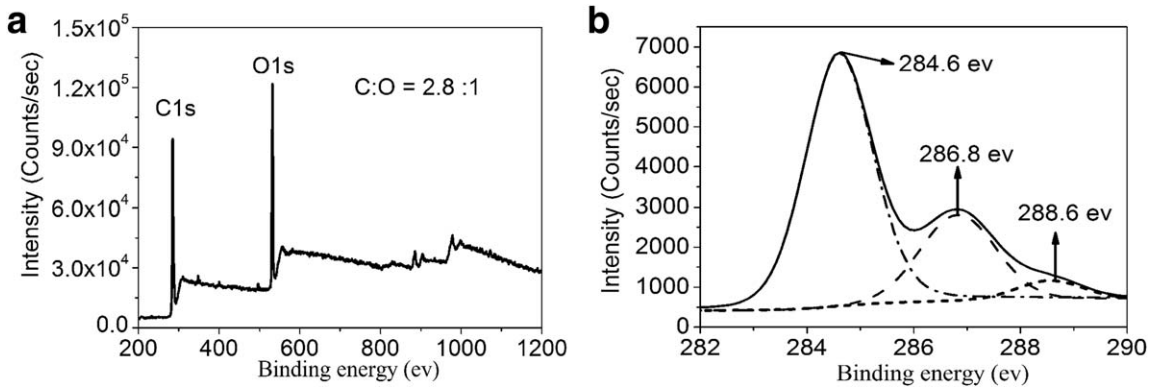

Figure 3. XPS spectra of GO: (a) XPS survey spectrum; (b) C1s XPS spectra.

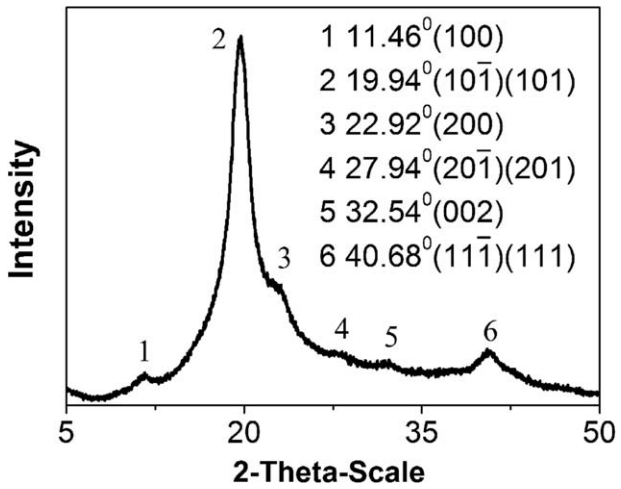

Figure 4. XRD pattern of PVA.

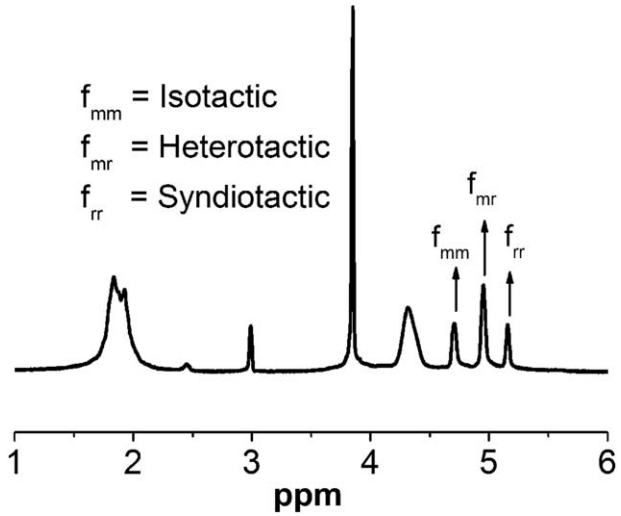

Figure 5. 1H NMR of PVA.

various parameters such as molecular weight, stereoregularity, and fillers.[4,23,24] The characteristic peak at 22.92° (Figure 4) indicates the PVA used here is atactic.[25] The three hydroxyl resonance lines in Figure 5 represent the isotactic (4.10 ppm), the herterotactic (4.33 ppm), and the syndiotactic (4.53 ppm) compositions of PVA, respectively, as reported previously.[26] The detailed compositions are 30.1%, 51.2%, and 18.4% for isotactic, herterotactic, and syndiotactic compositions, respectively.

Table I. Crystal Percentage and Melting Point

	First heating			Second heating
samples	T_p (°C)	% C	Half width (°C)	T_g (°C)
H-1	226.5	27.9	6.3	79.2
H-2	226.1	26.1	7.3	80.6
H-3	225.8	25.7	8.9	81.4

To investigate the interaction change, DSC was recorded to investigate the change of glass transition temperature (*Tg*) and crystallinity (Figure 6). The introduction of GO leads to a slight improvement in the glass transition temperature of PVA hydrogels, indicating that strong interaction exists between GO and amorphous PVA. Similar results were also observed by Yang and co-authors.[27] This may be originated from the polar groups of the GO (referring to XPS analysis) and hydroxyl groups of the PVA. PVA hydrogel crystallinity was obtained by dividing the real heat of melting hydrogels by the heat of melting a 100% crystalline PVA sample that is 138.6 $J \cdot g^{-1}$.[28] The results show that the crystallinity decreases after the introduction of GO (Table I), which may be because of the limitation of PVA crystallization caused by the improved interaction in amorphous domain.[29] Furthermore, the melting point of the composite hydrogels shifts to a lower temperature and the half width of melting peak becomes wider, indicating that GO can act as a heterogenous nucleating agent[30] and lead to more decentralized crystal size. The slight decline of the melting point may be because of a relative weak interaction within mixed PVA/GO crystal domains compared to the pure PVA crystal domains. This is because GO is amphiphilic and the hydrogen bonds between GO and PVA is not as strong as those within pure PVA. Therefore, the structural regularity of PVA/GO crystal may be lower than the pure PVA crystal. Figure 7 shows the estimated structure of PVA and PVA/GO hydrogels where GO is dispersed in both crystal and amorphous domains. After the loading of

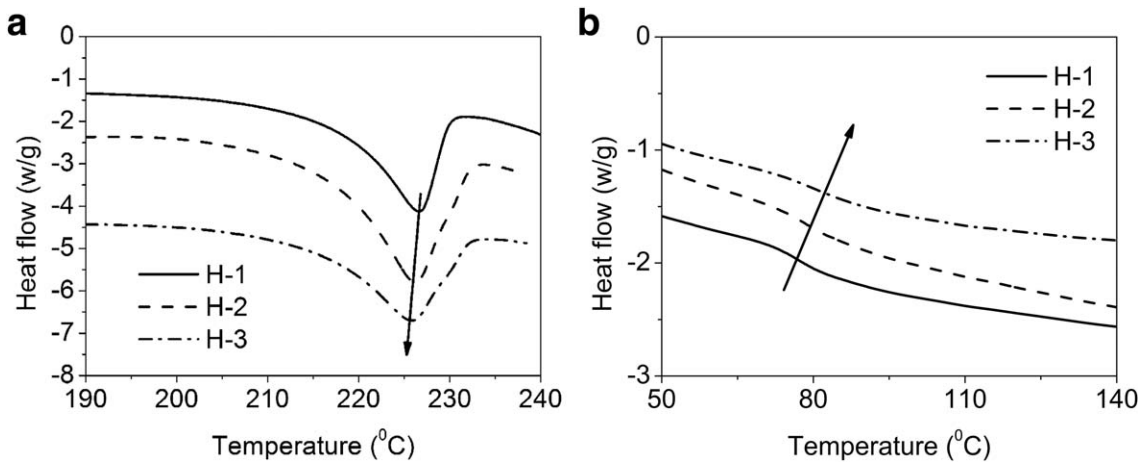

Figure 6. DSC curves: (a) first heating; (b) second heating.

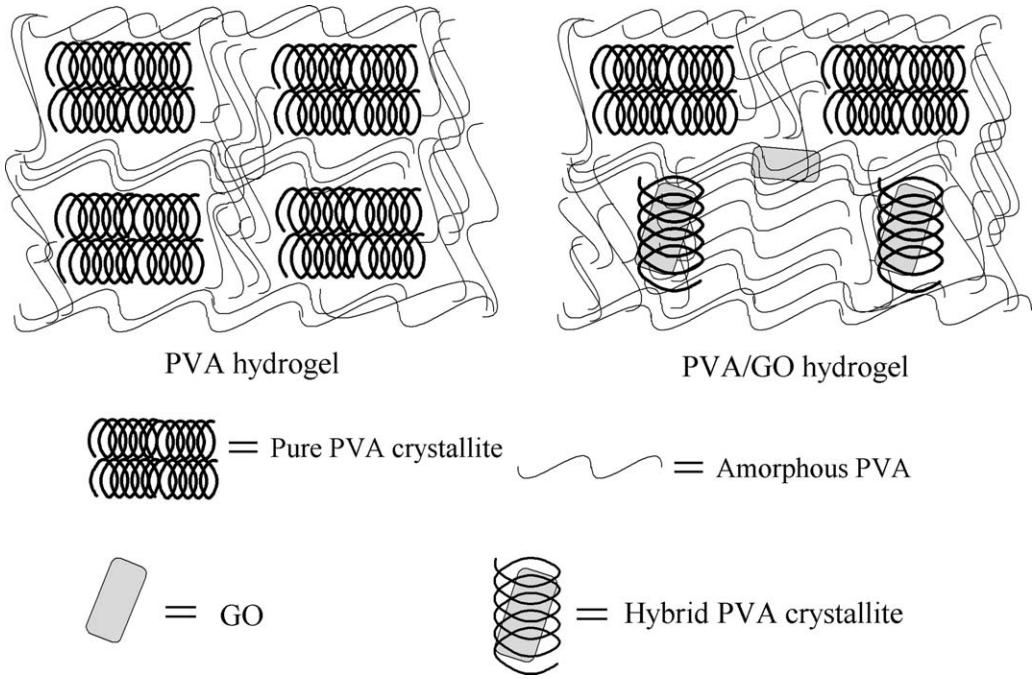

Figure 7. The schematic of PVA and PVA/GO hydrogels.

amphiphilic GO, the surface functional groups of GO may interact with the PVA molecules in amorphous area, leading to the improved interaction (Tg) and declined crystallinity. Meanwhile, GO in the crystal area may act as a nucleating agent, which lead to the imperfect crystal domain and more scattered crystal size.

Hydrogel swelling process can be affected by many factors such as hydrophilicity and hydrophobicity of the materials, and crosslinking and ionization degrees. Our experiment indicates that GO loading results in an enhanced swelling (Figure 8) and the hydrogel H3, the least crystalline structure, possesses the highest swelling ratio, because of the decreased crystalline.[31] Furthermore, polar groups such as carboxyl groups in GO may also facilitate the water diffusion, thus leading to enhanced swelling ratio. Our result here is slightly different from the swelling of PVA/hydrogels prepared by Zhang et al.[32] who reported that the introduction of a small amount of GO leads to an improved swelling, whereas further increase in GO restrains the swelling because of crosslinked hydrogen bonds between GO and PVA.

The adsorption isotherm of MB on hydrogels was measured under various initial MB concentrations ranging from 100 to 1000 mg/L. Hydrogels loaded with GO show notably improved adsorption capacity (Figure 9).

Langmuir and Freundlich models[7] are used to fit experimental data:

$$\frac{1}{q_e}=\frac{1}{q_m}+\frac{1}{bq_mc_e} \tag{4}$$

$$\ln q_e=\ln k_f+\frac{1}{n}\ln C_e \tag{5}$$

where q_e is the amount of adsorbed dye on the hydrogels at equilibrium time, C_e is the equilibrium liquid-phase concentrations of MB (mg/g). K_f is a function of adsorption energy and represents the adsorptive capacity.[33] The adsorption parameter n in the Freundlich isotherm refers to the adsorption intensity and high value of n indicates a strong bond between adsorbate and adsorbent.[34] The maximum adsorption capacity (q_m), Freundlich constant (K_f) and other parameters can be obtained by the linear fitting of the data. The fitting results indicate that the adsorption isotherms fit Freundlich model well with all correlation coefficient higher than 0.98 (Table II).

Introducing GO results in notable increase in both K_f and n (Table II), indicating that the interaction between cationic dye MB and PVA hydrogel is successfully enhanced. In previous reports, many methods such as sodium dodecyl sulphate gelation, introduction of clay and H^+ ionization have been used to improve the adsorption performances of hydrogels.[35–37] However, the improvement in the adsorption from the

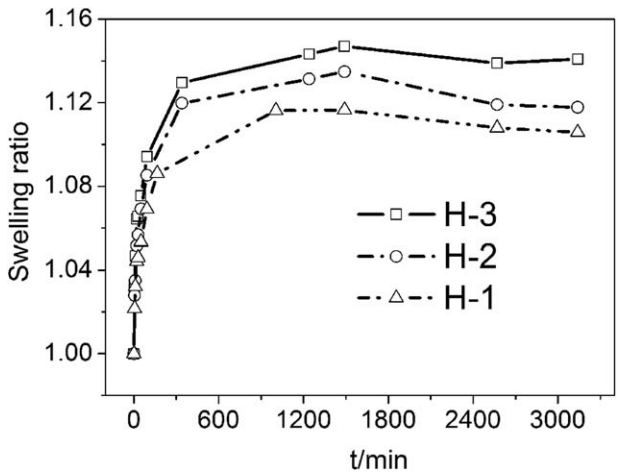

Figure 8. Swelling behaviors of hydrogels at 20°C.

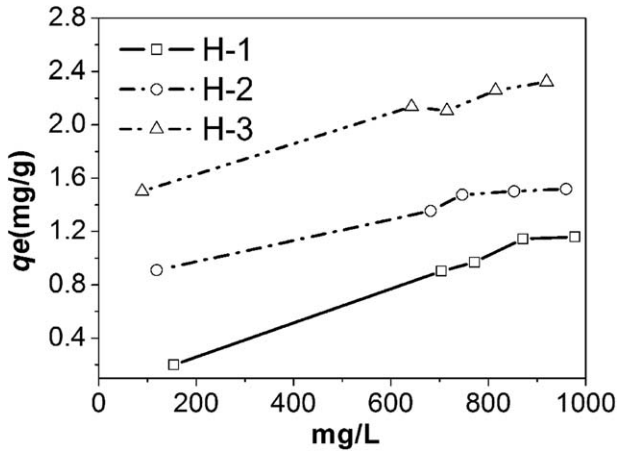

Figure 9. Absorption isotherm of MB on hydrogels at 25°C.

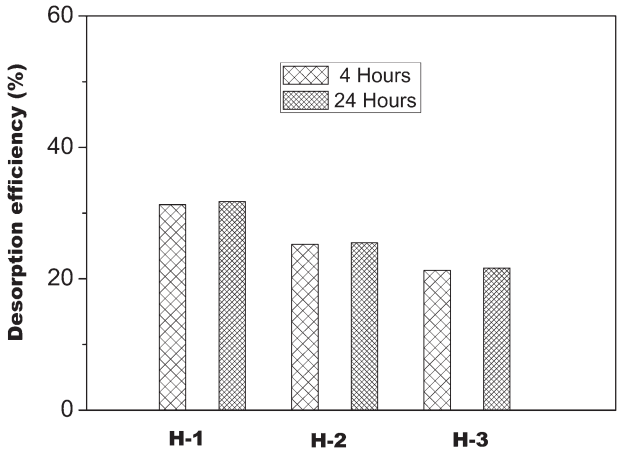

Figure 11. Desorption efficiency for MB at 20°C.

Table II. Frendich Isotherm Parameters for MB Absorption at 25°C

Hydrogel adsorbents	K_f [(mg g^{-1}) (dm^3 $mg^{-1})^{1/n}$)]	n	R^2
H-1	0.0015 ± 0.0003	1.02 ± 0.03	0.997
H-2	0.278 ± 0.028	4.02 ± 0.27	0.984
H-3	0.670 ± 0.008	5.56 ± 0.34	0.982

functionalized GO is more significant than those methods mentioned above, as demonstrated from the ratio of adsorptive capacities between the hydrogels with GO and without GO (Table III). For example, the adsorptive capacity for H3 is 446 times higher than that of the pure PVA hydrogel, which is much higher than that achieved from other methods.[35–37] The adsorption parameters n for hydrogels with GO show a similar improvement. This suggests the functionalized GOs in PVA

Table III. The Comparison of Freundlich Isotherm Constants Improvement Toward Cationic Dyes Reported from the Literature

Hydrogel adsorbents	Enhancer	Dyes	T (°C)	K_f'/K_{f0}[a]	n'/n_0[b]	R^2	References
H-2	0.3% GO	Methylene blue	25	185.3	3.91	0.984	Present study
H-3	0.6% GO	Methylene blue	25	446.7	5.42	0.982	Present study
Chitosan/sodium dodecyl sulphate hydrogel	Sodium dodecyl sulphate gelation	Methylene blue	30	6.84	1.59	0.925	[35]
Poly(methacrylic acid)/10% clay	10% clay	Crystal violet	30	1.10	1.03	0.963	[36]
Poly(methacrylic acid) /10% clay	10% clay	Methylene green	30	1.07	1.01	0.900	[36]
Poly(methacrylic acid) neutralization degree 0%	H^+ neutralization	Basic yellow 28	30	1.10	1.06	0.938	[37]

[a] K_f' and K_{f0} represent Freundlich isotherm constant (K_f) of the samples listed and the corresponding reference samples in different groups, respectively.
[b] n' and n_0 refer to Freundlich isotherm constants (n) of the samples listed and the corresponding reference samples, respectively, in each group.

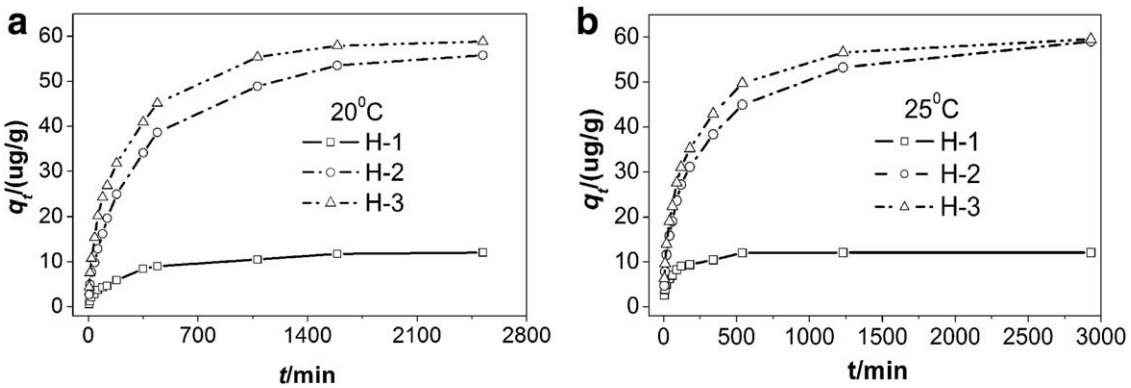

Figure 10. MB removal kinetics: (a) 20°C; (b) 25°C.

Table IV. Calculated Parameters of the Pseudo-Second-Order Kinetic Models

		q_e(μg g^{-1})				
Samples	T (°C)	Calculated	Experimental	k_2 (μg g^{-1}min^{-1})	R^2	$t_{0.5}$ (min)
H-1	20	12.63	12.01	5.19×10^{-4}	0.9987	105.4
	25	12.33	12.10	2.19×10^{-3}	0.9999	37.0
H-2	20	60.98	55.78	7.73×10^{-5}	0.9977	212.1
	25	62.15	59.05	1.14×10^{-4}	0.9987	141.1
H-3	20	62.00	58.85	1.26×10^{-4}	0.9992	128.0
	25	63.49	59.56	1.59×10^{-4}	0.9995	99.1

hydrogel provide a much improved dye removal ability than the PVA hydrogels.

MB adsorption kinetics is investigated at 20°C and 25°C at the very dilute MB solution (Figure 10). The rate constant of adsorption is determined from the pseudo-first-order[38]] and pseudo-second-order kinetic[39,40] models, respectively:

$$\ln(q_e - q_t) = \ln q_e - k_1 t \tag{6}$$

$$\frac{t}{q_t} = \frac{1}{k_2 q_e^2} + \frac{t}{q_e} \tag{7}$$

where q_e and q_t are the MB adsorbed (μg g^{-1}) at equilibrium and at time t, respectively. k_1 (min^{-1}) and k_2 (μg g^{-1}min^{-1}) are the adsorption rate constants for pseudo-first-order and pseudo-second-order kinetic models, respectively. The correlation coefficients are all higher than 0.99, indicating that the MB adsorption follows the second-order kinetic models well (Table IV). All the calculated equilibrium adsorption is very close to but a little lower than the experimental equilibrium adsorption (experimental maximum adsorption). This might be because of the unreached equilibrium time. It is worth mentioning that the equilibrium adsorptions of H3 and H2 are improved more than 300% comparing to the pure H1. However, the equilibrium adsorption of H3 (0.6% GO) is just a little higher than H2 (0.3% GO). The half-adsorption time $t_{0.5}$—is the time for the hydrogel to uptake half of MB at equilibrium. It shows that the high temperature is helpful for all the hydrogels to reach half equilibrium.

As the pseudo-first-order and pseudo-second-order kinetic models cannot indicate the adsorption mechanism, Morris–Weber model[41] was used to analyze its adsorption mechanism. Morris–Weber model usually deals with the intraparticle diffusion process:

Table V. Intraparticle rate constant for hydrogels

Samples	T (°C)	K_d (μg g^{-1} min$^{-0.5}$)	R^2	t (min)
H-1	20	0.43	0.997	440
	25	0.84	0.977	180
H-2	20	1.80	0.999	440
	25	2.12	0.988	540
H-3	20	2.28	0.994	440
	25	2.44	0.985	540

$$q_t = K_d \cdot t^{0.5} \tag{8}$$

where K_d is the intraparticle rate constant (μg g^{-1} min$^{-0.5}$).

The adsorption data in Figure 10 have been analyzed with eq. (8) and the results are shown in Table V. For all the adsorption processes, they follow the Morris–Weber model well for time over 180 minutes or more depending on the temperature and absorbents used. Therefore, the limiting step for MB adsorption is intraparticle diffusion.[42]

Desorption studies can provide direct insight into the overall adsorption mechanism. The desorption of MB mostly happens within the first 4 hours and becomes very slowly in the following 20 hours (Figure 11). Desorption in deionized water suggests the involvement of weak physisorption. However, the desorption efficiency is not high (no more than 32%), indicating that there are still chemisorptions involved.[43] This may be because of the hydrogen bonds existing between PVA macromolecules and MB. Moreover, the desorption efficiency of all samples decreases after the GO introduced, showing that there are stronger chemical interactions between PVA/graphene hydrogels and MB dye comparing to the pure PVA hydrogel. This is because of the π–π electron donor acceptor interactions originated from the benzene rings in both MB molecules and GO surface as well as the electrostatic attraction between the negative GO and cationic MB.[44]

CONCLUSIONS

Amphiphilic GO can interact with PVA macromolecules in both amorphous and crystal domains. This interaction leads to an improved T_g, decreased melting points, and improved half width. All these effects results in improved mobility of PVA macromolecules in PVA hydrogels. Because of improved mobility, both the swelling ratio and dye removal ability of PVA/GO hydrogel are enhanced. As for the MB removal, its adsorption kinetics follows the second-order kinetic models and the Morris-Weber model, and the controlling step of adsorption is the intraparticle diffusion. MB adsorption isotherm follows Freundlich model and the adsorption is heterogeneous. Desorption studies indicate that the interaction between PVA hydrogels and MB are both physisorption and chemisorption.

ACKNOWLEDGMENTS

The authors acknowledge the scientific and technical assistance of the Australian Microscopy & Microanalysis Research Facility at the RMIT University in Australia on XPS experimentation.

REFERENCES

1. Liu, K. M.; Li, Y. B.; Xu, F. L.; Zuo, Y.; Zhang, L.; Wang, H. A.; Liao, J. G. *Mater. Sci. Eng. C Biomimetic Supramol. Syst. 29*, 261, **2009**.
2. Edgren, D.; Zhu, P. C.; Struble, E.; Frame, R.; Zhang, Y. *J. Macromol. Sci. Part A-Pure Appl. Chem. 47*, 545, **2010**.
3. Cavalieri, F.; Chiessi, E.; Villa, R.; Vigano, L.; Zaffaroni, N.; Telling, M. F.; Paradossi, G. *Biomacromolecules 9*, 1967, **2008**.
4. Hassan, C. M.; Peppas, N. A. *Macromolecules 33*, 2472, **2000**.
5. Ozkahraman, B.; Acar, I.; Emik, S. *Clean Soil Air Water 39*, 658, **2011**.
6. Rodrigues, F. H. A.; Pereira, A. G. B.; Fajardo, A. R.; Muniz, E. C. *J. Appl. Polym. Sci. 128*, 3480, **2013**.
7. Shukla, N. B.; Madras, G. *J. Appl. Polym. Sci. 126*, 463, **2012**.
8. Rong, M. Z.; Zhang, M. Q.; Ruan, W. H. *Mater. Sci. Technol. Lond. 22*, 787, **2006**.
9. Qiu, J. J.; Wang, S. R. *J. Appl. Polym. Sci. 119*, 3670, **2010**.
10. Li, D.; Muller, M. B.; Gilje, S.; Kaner, R. B.; Wallace, G. G. *Nat. Nanotechnol. 3*, 101, **2008**.
11. Yang, S. T.; Chang, Y. L.; Wang, H. F.; Liu, G. B.; Chen, S.; Wang, Y. W.; Liu, Y. F.; Cao, A. N. *J. Colloid Interface Sci. 351*, 122.
12. Kim, F.; Cote, L. J.; Huang, J. X. *Adv. Mater. 22*, **1954**.
13. Pan, Y.; Wu, T.; Bao, H.; Li, L. *Carbohydr. Polym. 83*, 1908, **2011**.
14. Stankovich, S.; Dikin, D. A.; Piner, R. D.; Kohlhaas, K. A.; Kleinhammes, A.; Jia, Y.; Wu, Y.; Nguyen, S. T.; Ruoff, R. S. *Carbon 45*, 1558, **2007**.
15. Chandra, V.; Park, J.; Chun, Y.; Lee, J. W.; Hwang, I.-C.; Kim, K. S. *ACS Nano 4*, 3979, **2010**.
16. Zhao, M. F.; Liu, P. *Desalination 249*, 331, **2009**.
17. Kai, D.; Prabhakaran, M. P.; Stahl, B.; Eblenkamp, M.; Wintermantel, E.; Ramakrishna, S. *Nanotechnology 23*, **2012**.
18. Lin, H.-R.; Ling, M.-H.; Lin, Y.-J. *J. Biomater. Sci. Polym. Ed. 20*, 637, **2009**.
19. Li, C. P.; Feng, C. F.; Peng, Z.; Gong, W.; Kong, L. X. *Polym. Compos. 34*, 88, **2013**.
20. Chatterjee, S.; Lee, M. W.; Woo, S. H. *Carbon 47*, 2933, **2009**.
21. Shen, J. F.; Hu, Y. Z.; Shi, M.; Lu, X.; Qin, C.; Li, C.; Ye, M. X. *Chem. Mater. 21*, 3514, **2009**.
22. Marcano, D. C.; Kosynkin, D. V.; Berlin, J. M.; Sinitskii, A.; Sun, Z. Z.; Slesarev, A.; Alemany, L. B.; Lu, W.; Tour, J. M. *ACS Nano 4*, 4806, **2010**.
23. Sugiura, K.; Hashimoto, M.; Matsuzawa, S.; Yamaura, K. *J. Appl. Polym. Sci. 82*, 1291, **2001**.
24. Fujii, K.; Mochizuki, T.; Ukida, J.; Matsumoto, M. *J. Polym. Sci. B Polym. Phys. 1*, 697, **1963**.
25. Zhang, Z. H.; Mo, Z. S.; Zhang, H. F.; Wang, X. H.; Zhao, X. *J. Macromol. Chem. Phys. 204*, 1557, **2003**.
26. Van der Velden, G.; Beulen, J. *Macromolecules 15*, 1071, **1982**.
27. Yang, X.; Shang, S.; Li, L. *J. Appl. Polym. Sci. 120*, 1355, **2011**.
28. Abitbol, T.; Johnstone, T.; Quinn, T. M.; Gray, D. G. *Soft Matter 7*, 2373.
29. Zhu, Y. L.; Du, Z. J.; Li, H. Q.; Zhang, C. *Polym. Eng. Sci. 51*, 1770, **2011**.
30. Kim, H. M.; Lee, J. K.; Lee, H. S. *Thin Solid Films 519*, 7766, **2011**.
31. Xiao, C.; Yang, M. *Carbohydr. Polym. 64*, 37, **2006**.
32. Zhang, L.; Wang, Z. P.; Xu, C.; Li, Y.; Gao, J. P.; Wang, W.; Liu, Y. *J. Mater. Chem. 21*, 10399, **2011**.
33. Foletto, E. L.; Battiston, S.; Mazutti, M. A.; Jahn, S. L. *Chem. Eng. Commun. 200*, 1027, **2013**.
34. Auta, M.; Hameed, B. H. *J. Ind. Eng. Chem. 19*, 1153, **2013**.
35. Chatterjee, S.; Chatterjee, T.; Lim, S. R.; Woo, S. H. *Environ. Technol. 32*, 1503, **2011**.
36. Marandi, G. B.; Kermani, Z. P.; Kurdtabar, M. *Polym. Plast. Technol. 52*, 310, **2013**.
37. Panic, V. V.; Madzarevic, Z. P.; Volkov-Husovic, T.; Velickovic, S. J. *Chem. Eng. J. 217*, 192, **2013**.
38. Dogan, M.; Alkan, M.; Türkyilmaz, A.; Özdemir, Y. *J. Hazard. Mater. 109*, 141, **2004**.
39. Ho, Y. S.; McKay, G. *Process Biochem. 34*, 451, **1999**.
40. Zheng, Y.; Liu, Y.; Wang, A. *Chem. Eng. J. 171*, 1201, **2011**.
41. El-Kamash, A. M.; Zaki, A. A.; El Geleel, M. A. *J. Hazard. Mater. 127*, 211, **2005**.
42. Rodríguez, A.; García, J.; Ovejero, G.; Mestanza, M., *J. Hazard. Mater. 172*, 1311, **2009**.
43. Roy, A.; Adhikari, B.; Majumder, S. B. *Ind. Eng. Chem. Res. 52*, 6502, **2013**.
44. Li, Y.; Du, Q.; Liu, T.; Peng, X.; Wang, J.; Sun, J.; Wang, Y.; Wu, S.; Wang, Z.; Xia, Y.; Xia, L. *Chem. Eng. Res. Des. 91*, 361, **2013**.